Sensors and Actuators A 315 (2020) 112242

Contents lists available at ScienceDirect

Sensors and Actuators A: Physical

journal homepage: www.elsevier.com/locate/sna

On the performance analysis of gas-actuated peristaltic micropumps

Amirhesam Banejad [a,b,c,d], Seyed Ali Mousavi Shaegh [a,b,e,*], Elias Ramezani-Fard [a,b,c], Parisa Seifi [b,f], Mohammad Passandideh-Fard [c,d,**]

[a] Orthopedic Research Center, Mashhad University of Medical Sciences, Mashhad, Iran
[b] Laboratory of Microfluidics and Medical Microsystems, BuAli Research Institute, Mashhad University of Medical Sciences, Mashhad, Iran
[c] Department of Mechanical Engineering, Ferdowsi University of Mashhad, Mashhad, Iran
[d] Micro/Nanofluidics Laboratory (MNL), Ferdowsi University of Mashhad, Mashhad, Iran
[e] Clinical Research Unit, Ghaem Hospital, Mashhad University of Medical Sciences, Mashhad, Iran
[f] Department of Electrical Engineering, Ferdowsi University of Mashhad, Mashhad, Iran

ARTICLE INFO

Article history:
Received 3 May 2020
Received in revised form 5 July 2020
Accepted 30 July 2020

Keywords:
Microfluidics
Micropump
Peristaltic pumping
Membrane actuation
Performance analysis

ABSTRACT

In this study, we report on the performance analysis of peristaltic micropumps to understand the impact of affecting parameters on micropump actuation membrane and overall micropump operation. To this end, a thermoplastic micropump consisting of three interconnected actuation units made of Poly(methyl methacrylate) (PMMA) and thermoplastic polyurethane (TPU) film is designed and fabricated. The actuation membrane for liquid pumping is made of TPU film that is located between the liquid and the actuation chambers. The effects of actuation gas pressure and actuation frequency on micropump characteristics in terms of pumping flow rate, volumetric efficiency, and generated liquid pressure are studied. A maximum flow rate of 56.28 $\pm$ 1.47 μl/min is obtained using an actuation pressure and frequency of 50 kPa and 15 Hz, respectively. An experimental setup is designed and assembled to measure the actual pressure experienced by the actuation membrane at different actuation frequencies and gas pressures. It is found that the increase of actuation pressure leads to the increment of membrane oscillation amplitude with subsequent increase of pumping flow rate and volumetric efficiency. However, a further increase of actuation pressure beyond a threshold (50 kPa) leads to the decline of membrane oscillation amplitude that decreases the flow rate. Also, an image processing of the actuation membrane reveals that the increase of actuation frequency results in the continuous reduction of the oscillation amplitude of micropump membrane. Similar to actuation pressure, the increase of actuation frequency beyond a critical value (15 Hz) leads to the decline of flow rate. Our findings provide critical insights required for optimal design and operation of micropumps and finding a compromise between optimum pumping flow rates and operating conditions for on-chip pumping.

1. Introduction

Meeting the requirement of an accurate fluid delivery in a minute scale has led to the development of various designs of micropumps for deployment in microfluidic and lab-on-chip applications [1–3]. The use of micropump in drug delivery [4–7], chemical/biological applications [8,9], space explorations [10], and micro-electronics have introduced this microdevice as a key actuator in microfluidic systems. Many improvised concepts with various structures, actuation mechanisms, and manufacturing methods have been utilized to advance the micropump technology for different applications [1].

In general, micropumps could be classified into mechanical and non-mechanical ones. The mechanical micropumps employ an oscillating membrane, also known as diaphragm, which is actuated by an external power source to displace liquid for pumping purposes [11–13]. The mechanical micropumps are more frequently employed in different microfluidic applications including but not limited to lab-on-chip (LOC) devices [14,15], micro total analysis systems (μTAS) [16], DNA hybridization [17], fuel cells [18,19], and gas chromatography [20].

Mechanical micropumps mainly consist of a few interconnected actuation units for consecutive actuation of liquid. Each actua-

* Corresponding author at: Orthopedic Research Center, Mashhad University of Medical Sciences, Mashhad, Iran
** Corresponding author at: Department of Mechanical Engineering, Ferdowsi University of Mashhad, Mashhad, Iran.
E-mail addresses: mousavisha@mums.ac.ir (S.A. Mousavi Shaegh), mpfard@um.ac.ir (M. Passandideh-Fard).

https://doi.org/10.1016/j.sna.2020.112242
0924-4247/

Nomenclature

V	Volume (m^3)
R	Radius (m)
H	Height (m)
F	Frequency (Hz)
P	Pressure (kPa)
Q	Volumetric flow rate (μl/min)
N	Number of cycle
Greek Symbols	
η	Volumetric efficiency (%)
Subscripts	
Th	Theoretical
Exp	Experimental
sl	Swept Liquid

tion unit could include an actuation chamber, a liquid chamber, a membrane, and an actuation mechanism to actuate the membrane [1]. Amongst various mechanical micropumps, peristaltic types consisting of at least three units have been widely developed for microscale flow manipulations. This is mainly due to the high-precision and low-cost of peristaltic micropumps. Different actuation mechanisms including piezoelectric (PZT) [21], electromagnetic force [22], electrostatic force [20], thermospneumatics [23,24] and pneumatics [25,26] have been utilized to excite the membrane in peristaltic micropumps. In addition, other actuation mechanisms for pumping such as electro-osmosis have been explored theoretically [27–30], numerically and experimentally [31–36]. Different aspects of peristaltic flows including hydrodynamics and thermal characteristics have been studied recently [37,38]. In this paper, however, the focus is on the performance analysis of gas-actuated peristaltic micropumps.

Many investigations have been reported on the development and optimization of high-performance peristaltic micropumps through the modulation of micropump design and employed materials [23,25,39–46]. In general, the performance curves of gas-actuated micropumps demonstrate a peak in terms of pumping flow rate versus actuation pressure and actuation frequency. This characteristic is mainly associated with the behavior of actuation membrane and operating conditions; however, no detailed performance analysis of micropumps has been provided in the literature. In fact, a comprehensive understanding of membrane function and possible affecting uncertainties on its deformation is desired for optimization purposes.

In this research, the performance of a micropump actuating membrane is studied. In this way, a multi-layer pneumatic peristaltic micropump consisting of three interconnected actuation units is fabricated in PMMA, Fig. 1. A TPU film is employed as the actuation membrane due to its high elasticity and mechanical resilience. All layers are bonded using a low-pressure thermal fusion bonding method. The effects of actuation gas pressure and actuation frequency on the TPU membrane deformation are investigated through volumetric efficiency analysis and image processing approach. Importantly, to understand possible uncertainties associated with membrane actuation, a pressure measurement system is developed to quantify the actual gas pressure experienced by the TPU membrane at different gas actuation frequencies and gas pressures.

2. Experimental setup

2.1. Materials and apparatus

PMMA sheets (thickness of 2 mm, Calvin, Vietnam) are employed as the base material for fabricating various layers of the micropump. Due to the high rigidity of PMMA sheets, flexible thermoplastic polyurethane (TPU) (thickness of 25 μm, PT9200US NAT 1.0 mil, Covestro LLC, MA, USA) is utilized as an actuation membrane. TPU films have been investigated widely for biomedical purposes thanks to the specific properties of TPU such as biocompatibility and appropriate mechanical behaviors [47–49]. A 3D commercial computer numerical control (CNC) micromilling machine (DSP, China) with two flute flat endmills with diameters of 0.3 and 1 mm, is used to drill the desired features on the PMMA sheets. The SOLIDWORKS® (Version 2017) software is used to design the desired features. The Mastercam® software (Version 2017) is utilized to convert computer-aided design (CAD) files, exported by the SOLIDWORKS®, into an appropriate format for the micromilling machine. A laboratory vacuum oven (AFE200LV-60DH, ATRA, IRAN) connected to a vacuum pump (VE135 N, VALUE®, China), is employed for the thermal treatment and bonding procedure. An oil-free air compressor is used to produce pressurized air to actuate the TPU membranes of the micropump.

Three solenoid pneumatic switch valves (FESTO®, MH1-24 V DC) are used to control the actuation frequency of the micropump. They are normally closed valves that have ON and OFF modes of operations. They allow gas to pass through once they are activated (ON mode). In this way, pressurized gas in the control chamber over the membrane can deform the membrane. Once the valves are closed (OFF mode), the pressurized gas in the control chamber is released into the atmosphere and membrane restores its original flat shape.

A controller system (WAGO®, Fieldbus controller, System 750), equipped with the CODESYS® software, is utilized to handle the operation of pneumatic switch valves. The fabricated micropump is connected to the pneumatic switch valves with the aid of Tygon® tubes. For the flow rate measurement, deionized water mixed with red food dye with a volume ratio of 400:1 is used. A low-cost gas pressure sensor module (XGZP6887A, CfSensor, China) and an Arduino microcontroller (UNO R3, Italy) are employed to measure the real gas pressure that the membrane senses. The MATLAB® software is used for image processing purposes and also to interpret the received signals from the gas pressure sensor.

2.2. Design and fabrication of micropump

The multi-layer gas-actuated micropump includes three interconnected cylindrical liquid chambers, control chambers, actuation membranes, and inlet and outlet ports (Fig. 1a). The cylindrical liquid chambers with a diameter and height of 2 and 0.1 mm are interconnected through a rectangular liquid channel with a cross-section of 100*600 μm^2 (Fig. 1b). The control chambers are connected to the solenoid valves for pneumatic actuation of the TPU membranes. The introduction of compressed air into each control chamber through the switch valves pushes the actuation membrane downward leading to liquid movement. Liquid pumping is generated through the consecutive actuation of the membranes in a synchronized pattern. Different PMMA layers of the micropump are designed using SOLIDWORKS® software. The exported file from SOLIDWORKS® is then converted into G-code format with the aid of Mastercam® software. PMMA layers are fabricated using micromilling fabrication method [39]. TPU membranes are cut in desired dimensions using a sharp blade.

Prior to thermal fusion bonding for micropump fabrication, all prepared layers are initially washed with conventional water and

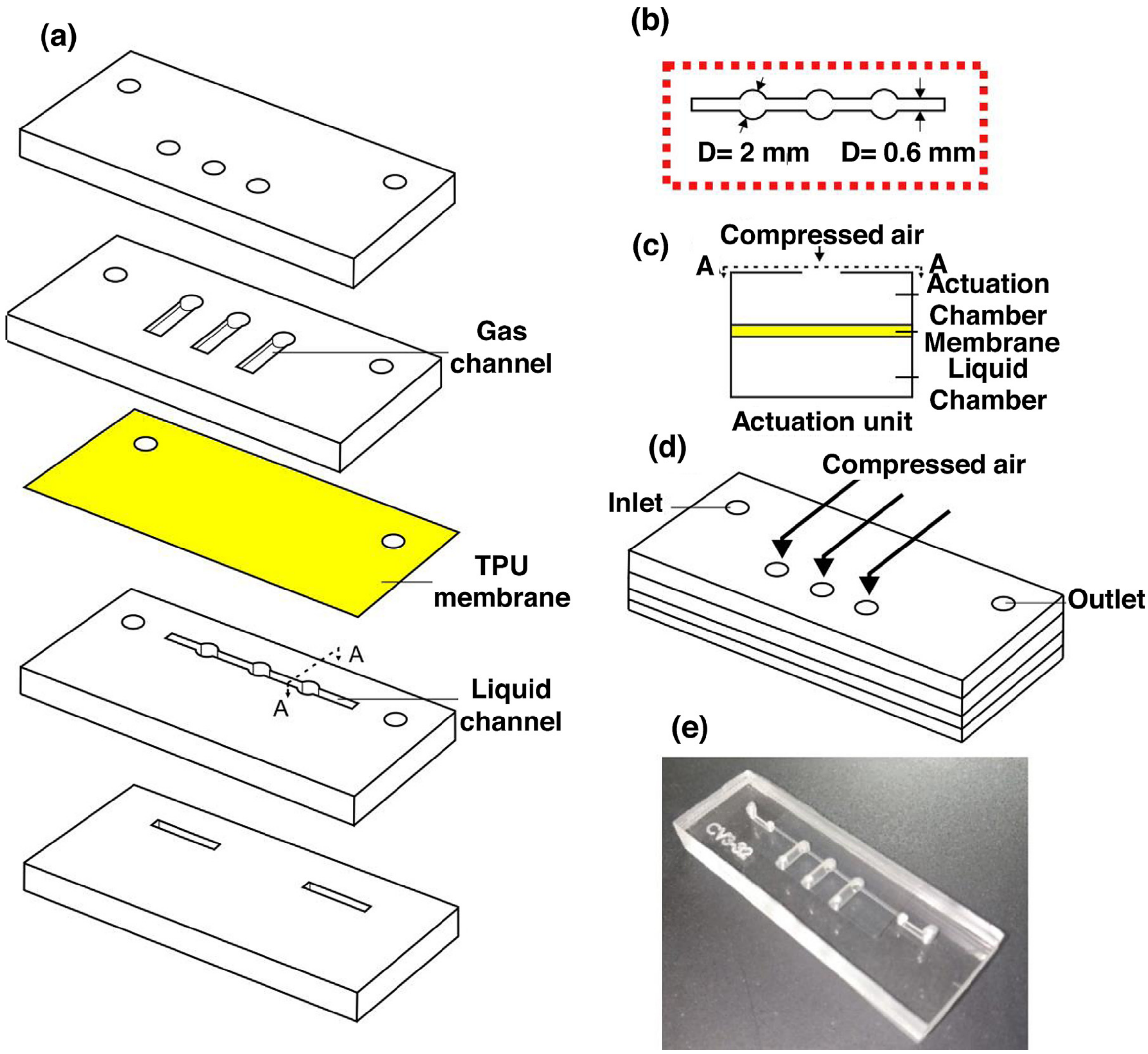

Fig. 1. Design and fabrication of the micropump. (a) A schematic illustration of the layers; (b) design of liquid channel (top view); (c) schematics of actuation unit of the micropump; (d) schematics of assembled micropump, and (e) image of the fabricated micropump.

soap. Then, they are kept in the oven at a temperature of 90 °C and an absolute pressure of 20 kPa (vacuum pressure of 80 kPa) for at least 8 h, followed by a gradual cooling to room temperature in approximately 50 mins. Afterward, all layers are assembled and sandwiched using paper clips and glass slides, while being kept in the oven at 145 °C and 20 kPa (vacuum pressure of 80 kPa) for 60 min. Finally, the layers are cooled to room temperature in about 50 min [39]. The assembled and fabricated micropump is shown in Fig. 1d and e.

To actuate the membrane for liquid pumping in a cyclic operation, a 6-stage actuation pattern is employed to control the ON-OFF operation of the solenoid valves (Fig. 2) [50]. The ideal performance of the micropump occurs once the liquid in each cylindrical liquid chamber is swept completely during a cycle. For a peristaltic micropump consisting of *n* chambers working based on the above-mentioned actuation pattern, the ideal volume of swept liquid in one cycle is:

$$V_{sl} = (n-2) * V \tag{1}$$

where V is the volume of a chamber. For a cylindrical chamber, therefore, the volume of swept liquid in each cycle is:

$$V_{sl} = \pi r^2 h \tag{2}$$

where *r=1 mm* and *h=100* μm are the radius and height of the cylinder, respectively.

2.3. Test setup

Two experimental setups for the characterization of micropump operation and the measurement of actuation gas pressures are designed in this study as explained in the following sections.

2.3.1. Experimental setup for micropump operation

The experimental setup consists of a PC, a controller, solenoid switch valves, an oil-free air compressor, a pressure regulator and the fabricated micropump chip. The solenoid switch valves connected to the air compressor, are actuated with a controller which is commanded by CODESYS® software via a PC interface. The switch valves have a synchronized operation (Fig. 3). The pressure of compressed air supplied by the compressor is adjusted through a pressure regulator before the valves.

The operation of the micropump is studied when both upstream and downstream liquid pressures are set at atmospheric pressure. In this way, the inlet port of the micropump is connected to the liquid reservoir exposed to the atmosphere and the outlet port of the micropump is in contact with atmospheric pressure via a measurement tube (Tygon tube, Cole-Parmer, an inner diameter of 0.020

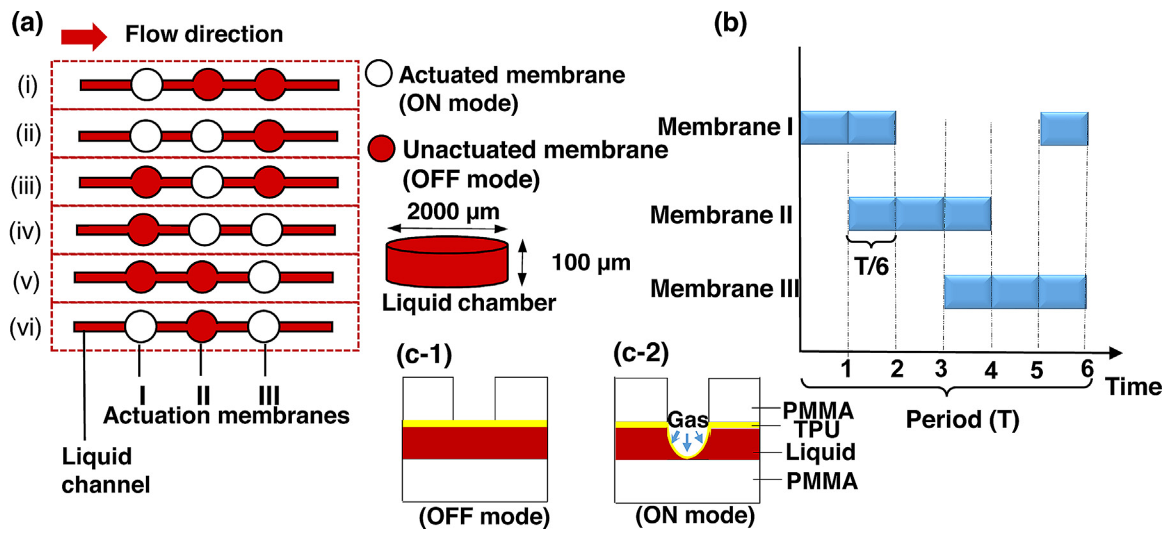

Fig. 2. (a) Schematic illustration for consecutive actuation of the micropump actuation units from top view, dimensions not to scale; (b) actuation time intervals for each actuation membrane; (c) cross sectional view of an actuation unit for OFF and ON modes.

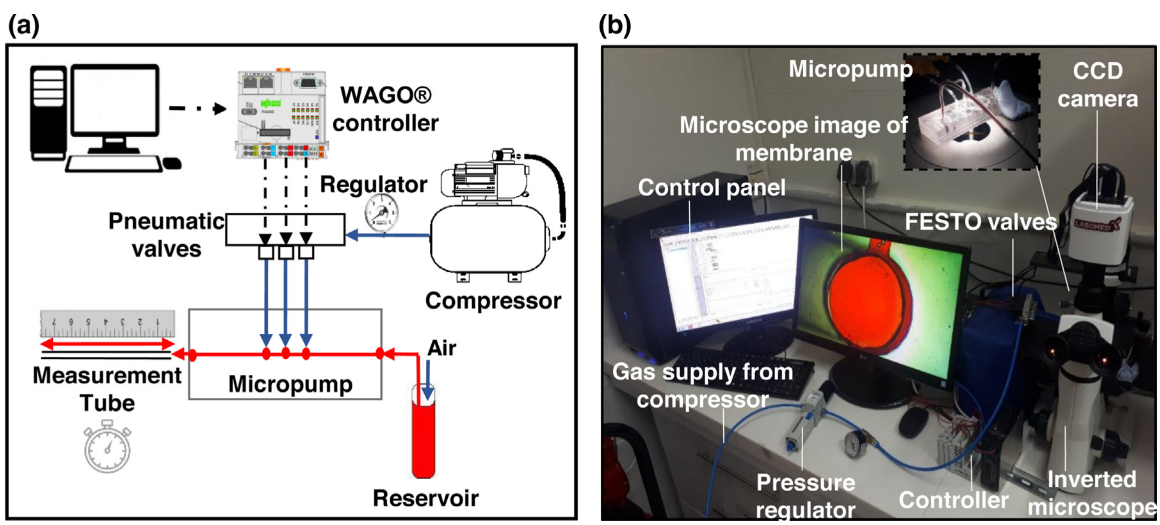

Fig. 3. (a) Schematics of the micropump test setup; (b) image of micropump test setup.

inch). The pumping rate is obtained by measuring the time needed to fill a certain volume of the measurement tube [44,51]. To investigate the effect of downstream pressure on the performance of the micropump, a liquid column with an adjustable height is connected to the outlet port. For different heights of the liquid column, the flow rates are measured.

2.3.2. Experimental setup for the gas pressure measurement

Fig. 4 shows an in-house designed and assembled test setup to measure the gas pressure applied over the membrane for actuation purposes. To this end, the low-cost piezoresistive pressure sensor module and the Arduino Uno microcontroller board with an ATmega 328 P microcontroller are utilized. The output of the pressure sensor is in analogue format; therefore, the analogue pins of the microcontroller is used to receive signals. The pressure sensor has an ability to measure the gauge pressure of non-corrosive gas or liquid ranged from 0 to 100 kPa. The analogue signals from the pressure sensor are recorded by the microcontroller every 1 ms. The signals are then transferred to a computer via a serial interface through a USB connection and are plotted using the MATLAB® software. To convert the signals into pressure values, a polynomial equation, obtained from a calibration curve, is used.

3. Results and discussion

Initially, bonding strength of the fabricated micropump is tested. To this end, the micropump chip is immersed in a water bath, and air with 600 kPa pressure is introduced into the inlet port and the actuation units of the micropump. No bubble leakage is observed.

3.1. Micropump characterization

The gas pressure and gas actuation frequency are two key factors affecting the performance of the micropump. Fig. 5a shows the flow rate as a function of gas actuation pressure for three constant actuation frequencies of 1, 5 and 20 Hz. It is obvious that for all three cases, there is an optimum pressure of 50 ± 0.5 kPa for which the maximum flow rate is obtained. To obtain the optimum performance of the micropump, the range of gas pressure was selected from 10 to 150 kPa. For the range of frequency, applying a gas actuation frequency more than 20 Hz was not possible due to the technical limitation of the switch valves.

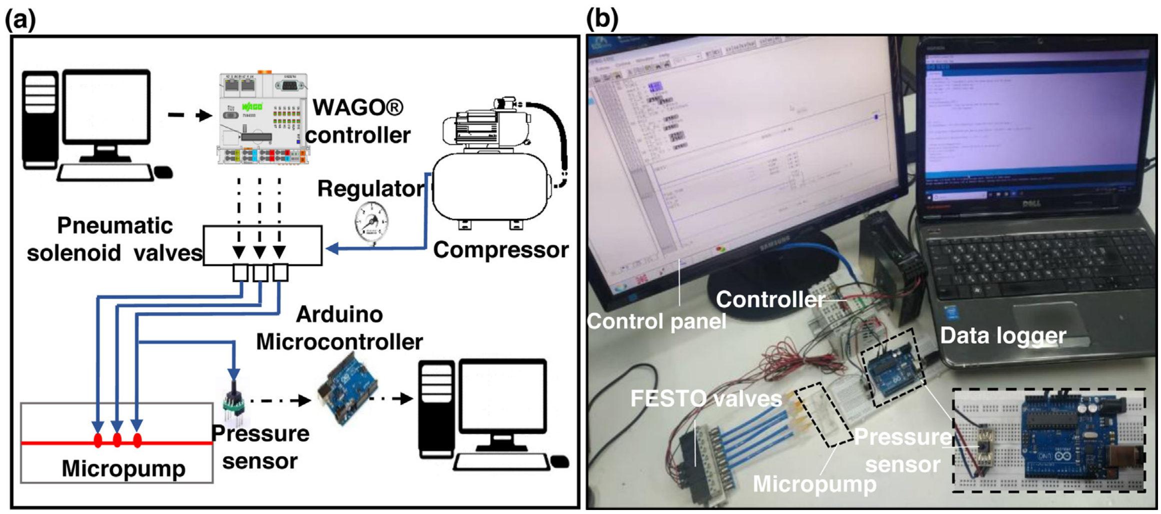

Fig. 4. (a) Schematics of gas measurement setup; (b) image of the experimental gas measurement setup.

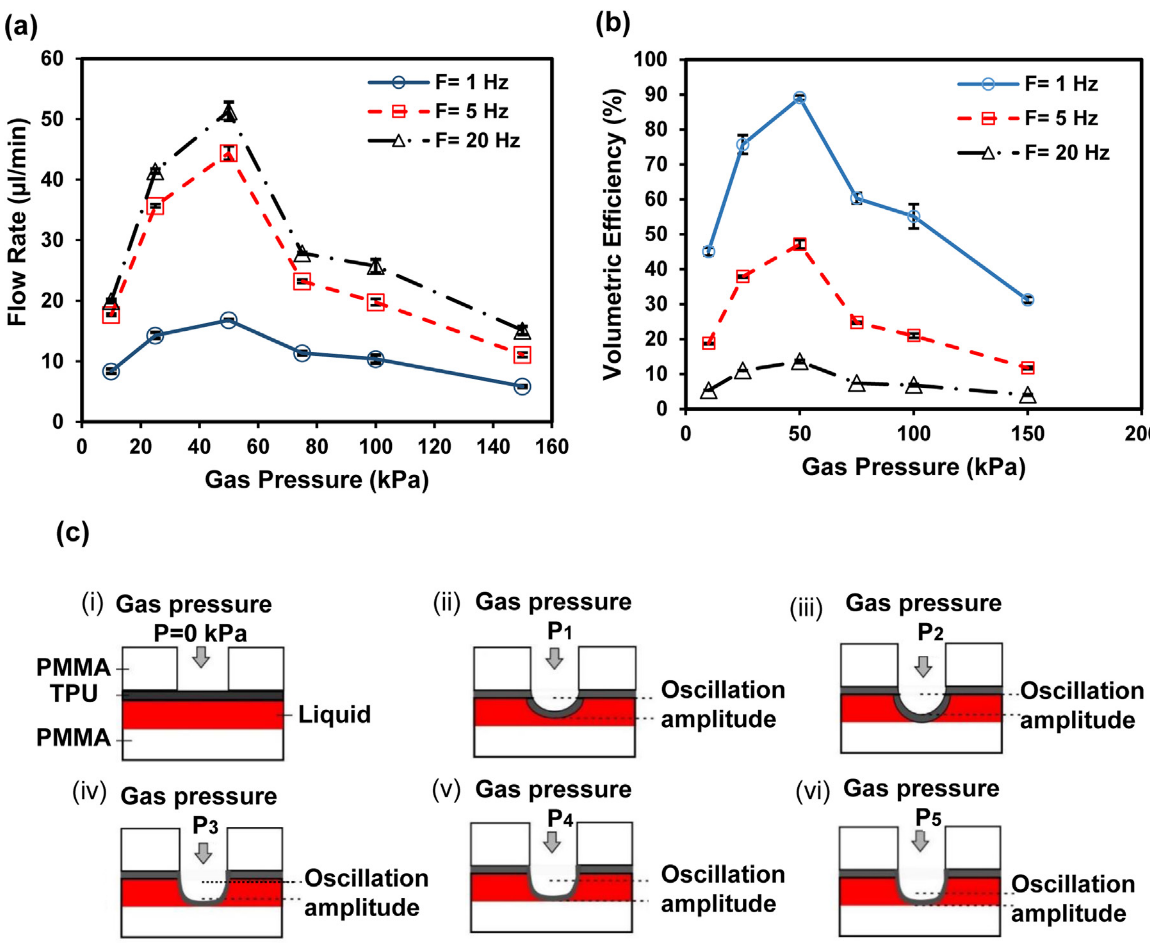

Fig. 5. (a) Flow rate versus gas pressure for three gas actuation frequencies of 1, 5 and 20 Hz; (b) volumetric efficiency versus gas pressure for three gas actuation frequencies of 1, 5 and 20 Hz; (c) schematic illustration showing variations of membrane oscillation amplitude at a constant actuation frequency as actuation pressure increases. Actuation pressure increases to P_5.

To characterize the pumping performance, the volumetric efficiency of micropump (η) is defined as [52]:

$$\eta = \frac{Q_{Exp}}{Q_{Th}} \quad (3)$$

where Q_{Exp} is the measured flow rate of the fabricated micropump, and Q_{Th} is the ideal flow rate of the micropump calculated as:

$$Q_{Th} = V_{sl} * F \quad (4)$$

In this equation, *Vsl* and *F* are the volume of swept liquid in each cycle, and the gas actuation frequency, respectively. Fig. 5b demon-

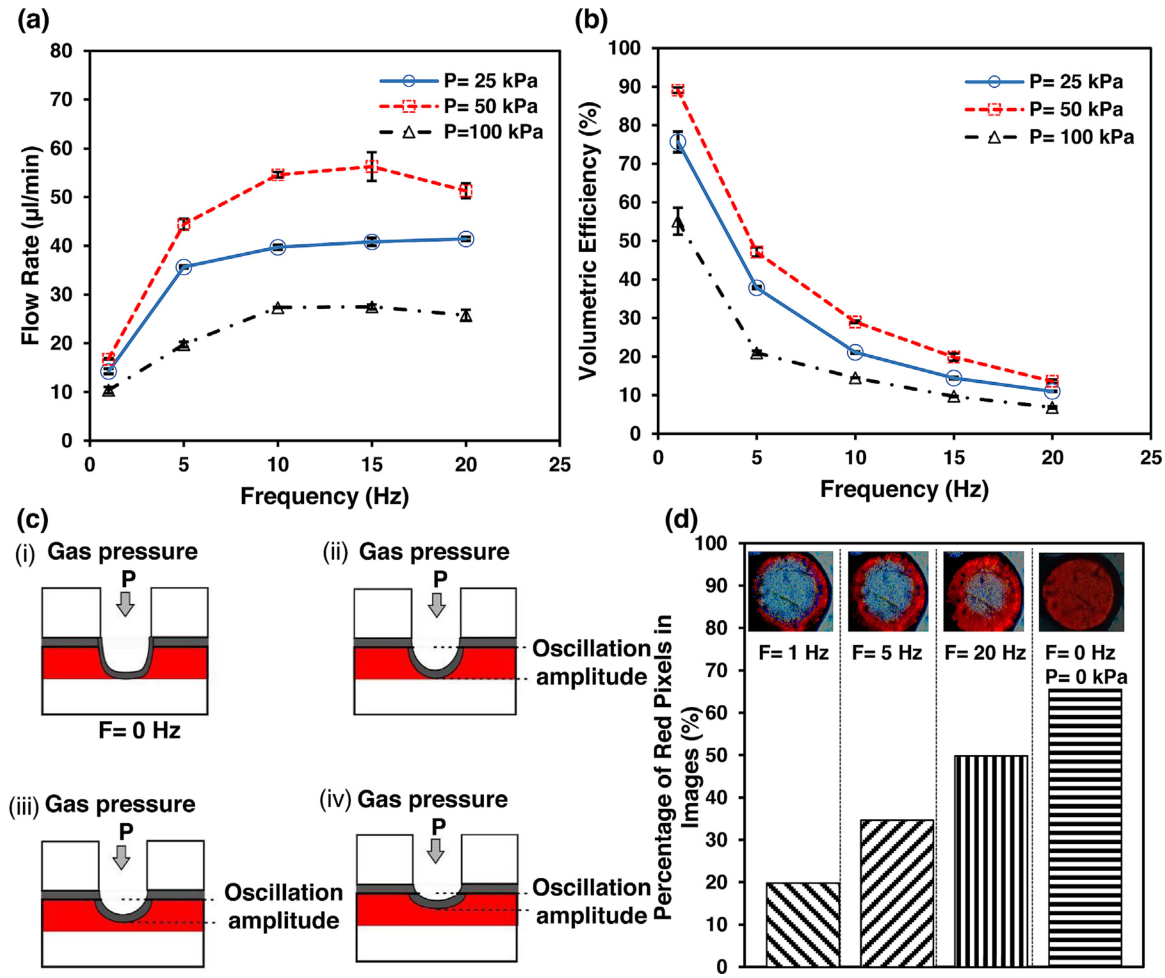

Fig. 6. (a) Flow rate versus frequency for three gas pressures of 25, 50 and 100 kPa; (b) volumetric efficiency versus frequency for three gas pressures of 25, 50 and 100 kPa; (c) schematic illustration of membrane oscillation amplitude at a constant actuation pressure as actuation frequency increases. Increasing the actuation frequency from (i) to (iv) reduces the oscillation amplitude; (d) membrane channel coverage for actuation frequencies of 1, 5, and 20 Hz and percentage of channel surface area with red color obtained from image processing. The black/red color indicates liquid in the liquid chamber (below the membrane) (For interpretation of the references to colour in this figure legend, the reader is referred to the web version of this article).

strates the variation of volumetric efficiency versus gas actuation pressure for three frequencies of 1, 5, and 20 Hz. Similar to Fig. 5a, the volumetric efficiency is maximum at a gas pressure of 50 kPa for the three cases. However, the volumetric efficiency is higher at a lower gas actuation frequency. For the frequency of 1 Hz, while the micropump flow rate is minimum (Fig. 5a), the corresponding volumetric efficiency is maximum (Fig. 5b). This behavior of the micropump might be explained as follows.

Once the actuation gas pressure is applied, the membrane moves downward to push the liquid as demonstrated in Fig. 5c-ii. With the increase of gas pressure, the membrane oscillation amplitude is increased. When the center point of the membrane reaches its maximum deflection to cover the whole channel height (Fig. 5c-iii), further increase of gas pressure leads to the deflection of the membrane to the peripherals resulting in a higher coverage of the liquid channel by the membrane (Fig. 5c-iv). Thus, more liquid volume is displaced per each cycle causing the increase of flow rate. Applying a higher gas pressure at a fixed frequency, however, has another effect on the oscillation amplitude of the membrane. For a fixed frequency, as the gas pressure increases, the membrane requires a longer time period to returns to its original position. This means that increasing the gas pressure will decrease the oscillation amplitude of the membrane (Fig. 5c-v and c-vi). It results in a decrease of the micropump flow rate and volumetric efficiency (Supplementary APPLICATION 1).

Fig. 6a and b illustrate the flow rate and volumetric efficiency versus actuation frequency for three different gas actuation pressures. Fig. 6a reveals that a higher flow rate is obtained at a gas pressure of 50 kPa (see also Fig. 5a). For all gas pressures, increasing the gas frequency increases the flow rate up to a certain point (15 Hz) after which the frequency has no significant effect. Fig. 6b reveals that with an increase of gas actuation frequency, the volumetric efficiency decreases (see also Fig. 5b) for three gas actuation pressures. The rate of reduction of the volumetric efficiency, however, is higher at lower frequencies. This micropump behavior could be associated with the membrane deflection at different actuation frequencies. As shown in Fig. 6c, at a fixed gas pressure, an increase of the actuation frequency reduces the oscillation amplitude of the membrane resulting in a continuous decrease of the volumetric efficiency. As displayed in Fig. 6b, however, the flow rate does not follow the same pattern. By increasing the frequency, the flow rate is also increased to a certain point. This originates from the fact that by increasing the gas actuation frequency, although the liquid volume swept per each cycle is reduced, the number of displaced volumes in one second increases, which in turn, leads to higher flow rate (Supplementary APPLICATION 2).

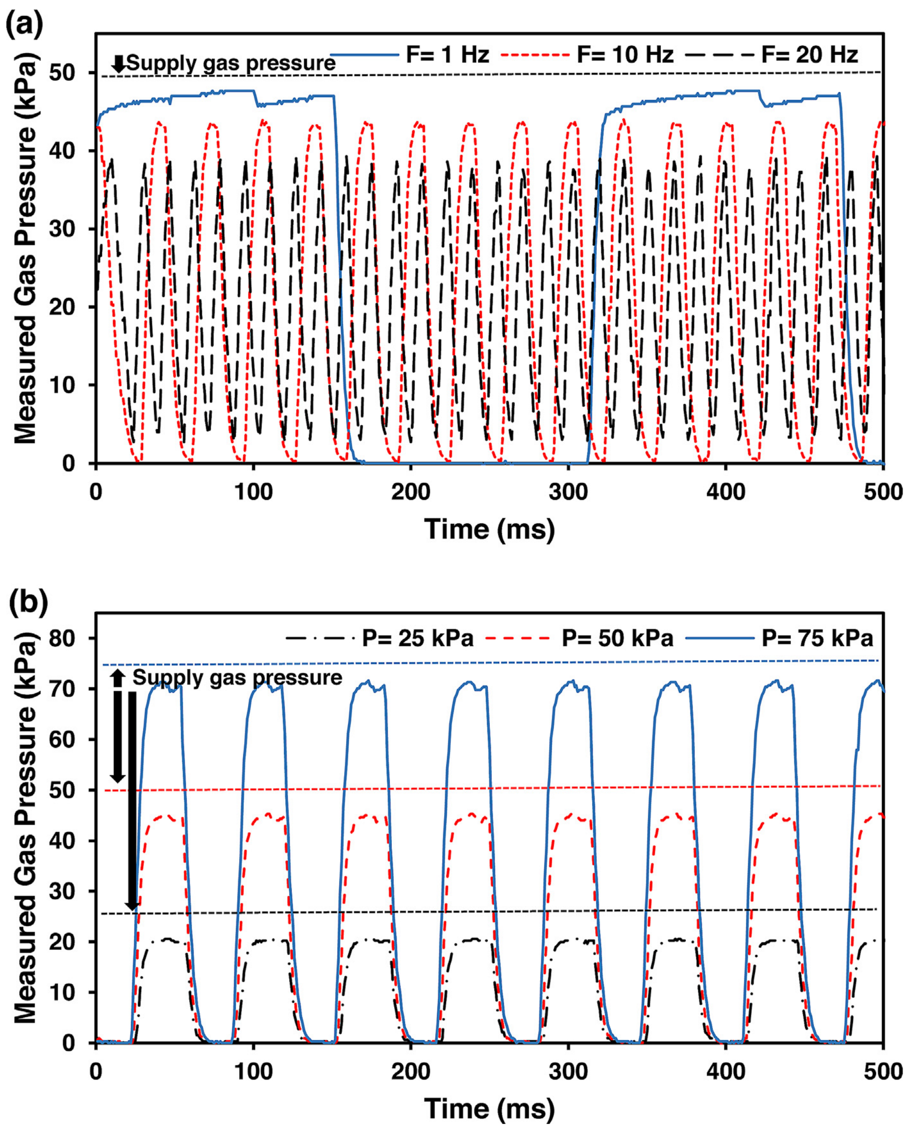

Fig. 7. Measured gas pressure in the actuation chamber above the membrane, (a) at a constant actuation supply pressure of 50 kPa for actuation frequencies of 1 Hz, 10 Hz, 20 Hz, and (b) at a constant actuation frequency of 5 Hz for supply gas pressures of 25 kPa, 50 kPa and 75 kPa.

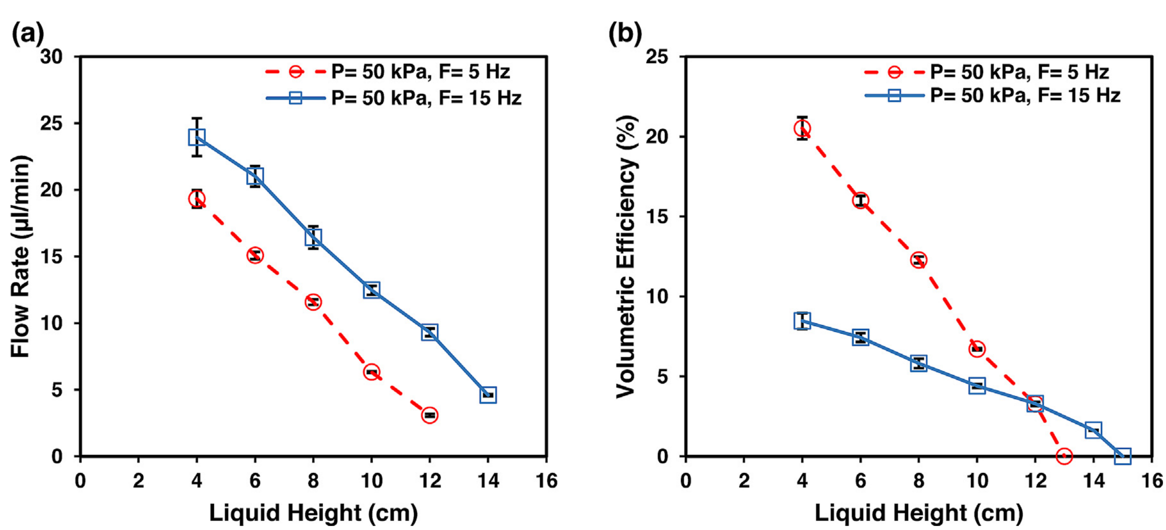

Fig. 8. (a) The impact of outlet liquid height on the pumping flow rate; (b) the impact of outlet liquid height on the volumetric efficiency of the micropump.

Eventually, the maximum volumetric efficiency of 89.09 % is obtained using a gas pressure of 50 kPa and an actuation frequency of 1 Hz. Meanwhile, the minimum volumetric efficiency (4%) is observed at 150 kPa and 20 Hz. Moreover, the maximum generated flow rate of 56.28 ± 1.47 μl/min is obtained at 50 kPa and 15 Hz. It should be noted that by increasing the density and viscosity of pumping liquid, higher gas pressure is required for pumping purposes to overcome friction losses.

Image processing of the membrane deformation at different frequencies revealed that the coverage of the liquid chamber with the membrane decreases as the actuation frequency increases from 1 Hz to 20 Hz. It indicates that the oscillation amplitude of the membrane decreases as the actuation frequency increments. The image processing is performed using the MATLAB® software to determine liquid percentage below the membrane during the actuation process as displayed in Fig. 6d. A code is commanded in the MATLAB® software to count pixels in a wide spectrum of red color through the elimination of other colors from the images. The intensity of red color increases from 19.8 % at a frequency of 1 Hz to 49.86 % at a frequency of 20 Hz meaning a decline of channel coverage by the membrane.

To further investigate the membrane deflection, the actuation pressure experienced by the membrane is measured. Fig. 7a presents the variations of gas pressure during micropump operation for three actuation frequencies of 1, 5, and 20 Hz once the pressure of gas supply for the membrane actuation is set on 50 kPa using a regulator. As the actuation frequency increases, the maximum value of gas pressure experienced by the membrane declines leading to the reduction of channel coverage. As the gas actuation frequency reaches 20 Hz, the maximum value and the oscillation amplitude of the gas pressure are decreased. The maximum and minimum values of gas pressures at this frequency are measured to be 39.29 kPa and 2.73 kPa, respectively. This behavior at a high frequency may be explained by the fact that there is not sufficient time for the pressurized gas to reach above the membrane in ON-mode actuation. Thus, the membrane deflection cannot cover the whole height of the liquid channel. Furthermore, in the OFF-mode actuation, with an increase of actuation frequency, the gas in the control chamber cannot be released completely into the atmosphere and, therefore, the membrane cannot restore its original flat shape. In this way, the amplitude of membrane oscillation is limited to only a fraction of the channel height leading to a decrease of the liquid volume swept by the membrane. Variations of gas pressure over the actuation membrane for two different supply gas pressures and a fixed actuation frequency of 5 Hz are also measured. Fig. 7b shows that the experienced pressure by the membrane is lower than the supply gas pressure. For actuation pressures of 25 kPa, 50 kPa and 75 kPa, the pressures over the membrane are measured as 20.6 kPa, 45.3 kPa and 71 kPa, respectively. This difference could be related to pressure drop through tubing and switch valves.

As a final step, the effect of downstream pressure on the operation of the membrane is also studied. To this end, a gas pressure of 50 kPa with two gas actuation frequencies of 5 and 15 Hz are selected as working conditions. As shown in Fig. 8a, when the liquid height (downstream pressure) is increased, the flow rate is decreased with a nearly constant slope. Furthermore, the rise of gas actuation frequency increases the liquid height of the micropump at the outlet port. For a gas pressure of 50 kPa and a frequency of 15 Hz, as the liquid height rises from 4 cm to 14 cm, the overall pumping flow rate decreases from 23.95 to 4.59 μl/min. For this working condition, the obtained maximum liquid height is approximately 15 cm meaning that the micropump can provide a liquid pressure of about 1.5 kPa (by neglecting the effects of friction loss and capillarity). The volumetric efficiency of the micropump in such working conditions is calculated (Fig. 8b). The volumetric efficiency for the gas actuation frequencies of 5 and 15 Hz are calculated to be 20.52 % and 8.47 %, respectively, at a liquid height of 4 cm (i.e. downstream pressure $\approx$ 0.4 kPa) that are followed by consistent reduction. As shown in Fig. 8b, for both gas actuation frequencies, with an increase of the liquid height, the volumetric efficiency decreases meaning a reduction of displaced liquid in each cycle.

4. Conclusions

In this paper, we report the performance analysis of gas-actuated peristaltic micropumps for optimization purposes. To this end, a micropump consisting of three interconnected actuation units is fabricated using PMMA sheets and TPU films. The micropump is characterized at different working conditions of gas actuation pressure and frequency. It is found that pumping flow rate versus actuation pressure and actuation frequency show peak value that is mainly associated with membrane behavior. It is revealed that the increase of actuation gas pressure at a fixed actuation frequency has two opposing effects on the micropump performance. Increment of actuation pressure induces higher channel coverage by the membrane leading to an increase of liquid volume swept by membrane per cycle. However, applying excessive actuation pressure decreases the oscillation amplitude of the membrane resulting in a negative impact on the flow rate. Similar to the effect of actuation pressure on flow rate, an increase of actuation frequency enhances the pumping flow rate. However, after a certain threshold, higher frequencies result in the decline of flow rate. The image processing approach reveals that this behavior is mainly related to shorter oscillation amplitude of the membrane once the actuation frequency rises. In this way, the volume of displaced liquid by the membrane actuation decreases as the frequency increases. To enhance membrane lifetime for long-term operations such as on-chip cell culturing for drug testing, a desired flow rate should be produced using the lowest actuation frequency and pressure that minimize cyclic membrane deflections.

Declaration of Competing Interest

The authors report no declarations of interest.

Acknowledgement

S.A.M.S. gratefully acknowledges funding by National Institute for Medical Research Development (NIMAD) under grant number 957144.

Appendix A. Supplementary data

Supplementary material related to this article can be found, in the online version, at doi:https://doi.org/10.1016/j.sna.2020.112242.

References

[1] S. Mohith, P.N. Karanth, S. Kulkarni, Recent trends in mechanical micropumps and their applications: a review, Mechatronics 60 (2019) 34–55.
[2] Y.-N. Wang, L.-M. Fu, Micropumps and biomedical applications – a review, Microelectron. Eng. 195 (2018) 121–138, http://dx.doi.org/10.1016/j.mee.2018.04.008.
[3] N.-T. Nguyen, S.T. Wereley, S.A.M. Shaegh, Fundamentals and Applications of Microfluidics, third ed., Artech house, 2019.
[4] A.H. Sima, A. Salari, M.B. Shafii, Low-cost reciprocating electromagnetic-based micropump for high-flow rate applications, J. Micro/Nanolithogr. Mems Moems 14 (2015), 035003.
[5] C. Mousoulis, et al., A skin-contact-actuated micropump for transdermal drug delivery, IEEE Trans. Biomed. Eng. 58 (2011) 1492–1498.
[6] W. Wei, S. Guo, A novel PDMS diaphragm micropump based on ICPF actuator, in: 2010 IEEE International Conference on Robotics and Biomimetics, IEEE, 2010.

[7] K. Junwu, et al., Design and test of a high-performance piezoelectric micropump for drug delivery, Sens. Actuators A Phys. 121 (2005) 156–161.
[8] P.C. Li, Microfluidic lab-on-a-Chip for Chemical and Biological Analysis and Discovery, CRC press, 2005.
[9] A.K. Au, et al., Microvalves and micropumps for BioMEMS, Micromachines 2 (2011) 179–220.
[10] R. Krpoun, H. Shea, Integrated out-of-plane nanoelectrospray thruster arrays for spacecraft propulsion, J. Micromech. Microeng. 19 (2009), 045019.
[11] D.J. Laser, J.G. Santiago, A review of micropumps, J. Micromech. Microeng. 14 (2004) 35–70.
[12] B.D. Iverson, S.V. Garimella, Recent advances in microscale pumping technologies: a review and evaluation, Microfluid. Nanofluidics 5 (2008) 145–174.
[13] F. Abhari, H. Jaafar, N.A.M. Yunus, A comprehensive study of micropumps technologies, Int. J. Electrochem. Sci. 7 (2012) 9765–9780.
[14] S.-M. Ha, W. Cho, Y. Ahn, Disposable thermo-pneumatic micropump for bio lab-on-a-chip application, Microelectron. Eng. 86 (2009) 1337–1339.
[15] N.A. Hamid, et al., A stack bonded thermo-pneumatic micro-pump utilizing polyimide based actuator membrane for biomedical applications, Microsyst. Technol. 23 (2017) 4037–4043.
[16] W. Zhang, R.E. Eitel, An integrated multilayer ceramic piezoelectric micropump for microfluidic systems, J. Intell. Mater. Syst. Struct. 24 (2013) 1637–1646.
[17] M. Saidur, A.A. Aziz, W. Basirun, Recent advances in DNA-based electrochemical biosensors for heavy metal ion detection: a review, Biosens. Bioelectron. 90 (2017) 125–139.
[18] B. Ong, S.K. Kamarudin, S. Basri, Direct liquid fuel cells: a review, Int. J. Hydrogen Energy 42 (2017) 10142–10157.
[19] J.Y. Hwang, et al., Periodic fuel supply to a micro-DMFC using a piezoelectric linear actuator, J. Micromech. Microeng. 20 (2010), 085023.
[20] S.Y. Jeong, et al., Peristaltic micropump with multi-electrodes using electrostatic force, in: Advanced Materials Research, Trans Tech Publ., 2015.
[21] T. Ma, et al., Piezoelectric peristaltic micropump integrated on a microfluidic chip, Sens. Actuators A Phys. 292 (2019) 90–96, http://dx.doi.org/10.1016/j.sna.2019.04.005.
[22] M. Rusli, et al., Electromagnetic actuation dual-chamber bidirectional flow micropump, Sens. Actuators A Phys. 282 (2018) 17–27.
[23] O.C. Jeong, et al., Fabrication of a peristaltic PDMS micropump, Sens. Actuators A Phys. 123 (2005) 453–458.
[24] B.T. Chia, H.-H. Liao, Y.-J. Yang, A novel thermo-pneumatic peristaltic micropump with low temperature elevation on working fluid, Sens. Actuators A Phys. 165 (2011) 86–93.
[25] O.C. Jeong, S. Konishi, Fabrication of a peristaltic micro pump with novel cascaded actuators, J. Micromech. Microeng. 18 (2008) 250–256.
[26] S.A.M. Shaegh, et al., Plug-and-play microvalve and micropump for rapid integration with microfluidic chips, Microfluid. Nanofluidics 19 (2015) 557–564, http://dx.doi.org/10.1007/s10404-015-1582-4.
[27] V. Narla, D. Tripathi, G.R. Sekhar, Time-dependent analysis of electroosmotic fluid flow in a microchannel, J. Eng. Math. 114 (2019) 177–196.
[28] A. Bandopadhyay, D. Tripathi, S. Chakraborty, Electroosmosis-modulated peristaltic transport in microfluidic channels, Phys. Fluids 28 (2016), 052002.
[29] N. Ranjit, G. Shit, D. Tripathi, Entropy generation and Joule heating of two layered electroosmotic flow in the peristaltically induced micro-channel, Int. J. Mech. Sci. 153 (2019) 430–444.
[30] V. Narla, D. Tripathi, O. Anwar Bég, Electro-osmosis modulated viscoelastic embryo transport in uterine hydrodynamics: mathematical modeling, J. Biomech. Eng. 141 (2019).
[31] J. Prakash, D. Tripathi, O.A. Bég, Comparative study of hybrid nanofluids in microchannel slip flow induced by electroosmosis and peristalsis, Appl. Nanosci. (2020) 1–14.
[32] V. Narla, D. Tripathi, O.A. Bég, Analysis of entropy generation in biomimetic electroosmotic nanofluid pumping through a curved channel with joule dissipation, Therm. Sci. Eng. Prog. 15 (2020), 100424.
[33] P. Jayavel, et al., Electroosmotic flow of pseudoplastic nanoliquids via peristaltic pumping, J. Braz. Soc. Mech. Sci. Eng. 41 (2019) 61.
[34] D. Tripathi, et al., Transient peristaltic diffusion of nanofluids: a model of micropumps in medical engineering, J. Hydrodynam. B 30 (2018) 1001–1011.
[35] J. Prakash, A.K. Ansu, D. Tripathi, Alterations in peristaltic pumping of Jeffery nanoliquids with electric and magnetic fields, Meccanica 53 (2018) 3719–3738.
[36] D. Tripathi, et al., Three-layered electro-osmosis modulated blood flow through a microchannel, Eur. J. Mech. B Fluids 72 (2018) 391–402.
[37] M. Bhatti, et al., Numerical study of heat transfer and Hall current impact on peristaltic propulsion of particle-fluid suspension with compliant wall properties, Mod. Phys. Lett. B 33 (2019), 1950439.
[38] M.M. Bhatti, et al., Hydrodynamics interactions of metachronal waves on particulate-liquid motion through a ciliated annulus: application of bio-engineering in blood clotting and endoscopy, Symmetry 12 (2020) 532.
[39] A. Banejad, et al., Design, fabrication and experimental characterization of whole-thermoplastic microvalves and micropumps having micromilled liquid channels of rectangular and half-elliptical cross-sections, Sens. Actuators A Phys. 301 (2020), 111713, http://dx.doi.org/10.1016/j.sna.2019.111713.
[40] S.A.M. Shaegh, et al., Rapid prototyping of whole-thermoplastic microfluidics with built-in microvalves using laser ablation and thermal fusion bonding, Sens. Actuators B Chem. 255 (2018) 100–109, http://dx.doi.org/10.1016/j.snb.2017.07.138.
[41] P.E. Guevara-Pantoja, et al., Pressure-actuated monolithic acrylic microfluidic valves and pumps, Lab Chip 18 (2018) 662–669, http://dx.doi.org/10.1039/C7LC01337J.
[42] J. Goulpeau, et al., Experimental study and modeling of polydimethylsiloxane peristaltic micropumps, J. Appl. Phys. 98-105 (2005), 044914.
[43] S. Huang, et al., Preparation of normally open microvalves with fluorinated ethylene propylene membrane and poly (methyl methacrylate) substrates, Microfluid. Nanofluidics 14 (2013) 329–335.
[44] A. Pourmand, et al., Fabrication of whole-thermoplastic normally closed microvalve, micro check valve, and micropump, Sens. Actuators B Chem. 262 (2018) 625–636, http://dx.doi.org/10.1016/j.snb.2017.12.132.
[45] W. Inman, et al., Design, modeling and fabrication of a constant flow pneumatic micropump, J. Micromech. Microeng. 17 (2007) 891.
[46] C.-W. Huang, S.-B. Huang, G.-B. Lee, Pneumatic micropumps with serially connected actuation chambers, J. Micromech. Microeng. 16 (2006) 2265.
[47] M.V. Pergal, et al., Structure and properties of thermoplastic polyurethanes based on poly (dimethylsiloxane): assessment of biocompatibility, J. Biomed. Mater. Res. A 102 (2014) 3951–3964, http://dx.doi.org/10.1002/jbm.a.35071.
[48] W.-I. Wu, et al., Polyurethane-based microfluidic devices for blood contacting applications, Lab Chip 12 (2012) 960–970, http://dx.doi.org/10.1039/C2LC21075D.
[49] E. Piccin, et al., Polyurethane from biosource as a new material for fabrication of microfluidic devices by rapid prototyping, J. Chromatogr. A 1173 (2007) 151–158, http://dx.doi.org/10.1016/j.chroma.2007.09.081.
[50] S.-B. Huang, et al., A membrane-based serpentine-shape pneumatic micropump with pumping performance modulated by fluidic resistance, J. Micromech. Microeng. 18 (2008) 450–468.
[51] B. Liu, et al., A rotary ferrofluidic vane micropump with C shape baffle, Sens. Actuators B Chem. 263 (2018) 452–458, http://dx.doi.org/10.1016/j.snb.2018.02.113.
[52] C.Y. Park, M. Shur, C.F. Dewey Jr., A study of fluid-membrane interactions that limit the output of peristaltic micropumps, J. Mech. Med. Biol. 11 (2011) 325–336.

Biographies

Amirhesam Banejad obtained a B.Sc. degree in 2016 from Bu-Ali Sina University, Hamedan, Iran, and a M.Sc. degree in 2019 from Ferdowsi University, Mashhad, Iran, both in Mechanical Engineering. His M.Sc. project was focused on the development of whole-thermoplastic microdevices. His research interests are the development of MEMS-based actuators, cancer diagnosis and microfluidics.

Seyed Ali Mousavi Shaegh received a B.S. and a M.S. in 2004 and 2007 from Yazd University, and Ferdowsi University of Mashhad, Iran, both in Mechanical Engineering. He received a Ph.D. in 2012 from Nanyang Technological University, Singapore, in Mechanical Engineering. He joined Harvard University, Brigham and Women's Hospital and Harvard-MIT Division of Health Sciences and Technology (HST), in 2014 as a postdoc fellow after a two-year research appointment at Singapore Institute of Manufacturing Technology (a research institute of Agency for Science, Technology and Research, A*STAR). Currently, he is an assistant professor at Mashhad University of Medical Sciences, in the School of Medicine. He is founder and director of Laboratory of Microfluidics and Medical Microsystems. Mousavi's research interests are mainly focused on microfluidic systems for diagnostics and drug testing, development of rapid prototyping methods for microfluidic chip fabrication, as well as design, fabrication, and testing of medical devices and implants.

Elias Ramezani-Fard received a B.Sc. degree in Mechanical Engineering from the Ferdowsi University of Mashhad (FUM) in 2019. In 2018, he joined Bone & Joint Research Lab as a research assistant to work on thermoplastic-based microfluidic devices. He started his M.Sc. program from 2019 at FUM with concentration on the development of high performance micropump based on diffuser/nozzle element. His research interests include development of microfluidics, cancer diagnosis and detection and separation of tumor cells.

Parisa Seifi received her B.Sc. degree in Biomedical Engineering (bioelectric) from Isfahan University, Isfahan, Iran in 2014 and a M.Sc. degree in Electrical Engineering of Sharif University of Technology, Tehran, Iran in 2016. She is currently a PhD student at the School of Electrical Engineering, Ferdowsi University of Mashhad doing a joined thesis with Mashhad University of Medical Sciences, Iran. Her research interests include nonlinear system control, stochastic control, adaptive control and controller design for microfluidic platforms.

Mohammad Passandideh-Fard obtained a B.Sc. degree in 1987 from Ferdowsi University of Mashhad, Mashhad, Iran and a M.Sc. degree in 1989 from Isfahan University of Technology, Isfahan, Iran both in Mechanical Engineering. He earned his Ph.D. in Mechanical Engineering from the University of Toronto, Toronto, Canada in 1998. Dr. Passandideh-Fard has been a professor at the Department of Mechanical Engineering, Ferdowsi University of Mashhad from 2004. His research interests includes modeling and experimentation on free surface flows, nanofluidics for heat transfer enhancement purposes and microfluidics.